The acoustical design and modelling of a subwavelength hexagonal acoustic metamaterial for multipurpose use and potential building applications[1]

Denilson Ramos[a*] | Francesco Pompoli[a] | Luís Godinho[b] | Paulo Amado-Mendes[b] | Paulo Mareze[c]

[a] Department of Engineering, University of Ferrara, Via Giuseppe Saragat, 1, 44124 Ferrara (FE)

[b] Institute for Sustainability and Innovation in Structural Engineering, University of Coimbra, Via Luis Reis dos Santos, 290, 3030-790 Coimbra

[c] Acoustical Engineering, Federal University of Santa Maria, Avenue Roraima, 1000, 97105-900 Santa Maria (RS)

* Corresponding author: dltdls@unife.it

Ricevuto: 5/2/2026
Accettato: 8/2/2026

DOI: 10.3280/ria2026oa22128
ISSNe: 2385-2615

The development and application of noise control strategies on subwavelength regimes have thus demanded a continuous effort by several researchers. In recent decades, the advent of acoustic metamaterials arose as a novel strategy on the sound wave manipulation and the development of subwavelength dimensions acoustic devices. In previous works by the authors, analytical approaches were developed to provide a more comprehensive acoustic characterization of the proposed metamaterial through equivalent fluid models. In contrast, the present work aims to advance the concept by introducing the design of a ventilated subwavelength acoustic metamaterial and by examining its potential applicability across multiple building-related contexts, including sound absorption and sound transmission control. By means of optimized geometrical configurations, it is possible to achieve quasi-perfect sound absorption (α > 0.8[-]) or enhanced sound transmission loss efficiency (> 30 [dB]) within subwavelength regimes. The results demonstrate that the proposed acoustic metamaterial operates effectively at subwavelength dimensions and within selectively tuned attenuation frequency bands, enabling single-, dual-, triple-, or hexa-resonance configurations. These features introduce additional degrees of freedom into the overall design concept, offering promising applications across various engineering fields, particularly in building acoustics.
Keywords: acoustic metamaterial, association of Helmholtz resonators, sound absorption, sound transmission loss, building acoustics

Progettazione e modellazione acustica di un metamateriale acustico esagonale sub-lunghezza d'onda per usi multifunzionali e potenziali applicazioni edili

Lo sviluppo e l'applicazione di strategie per il controllo del rumore in regimi sub-lunghezza d'onda (subwavelength) hanno richiesto un impegno costante da parte di numerosi ricercatori. In questo contesto, l'avvento dei metamateriali acustici si è presentato come una strategia innovativa per la manipolazione delle onde sonore e per lo sviluppo di dispositivi acustici dalle dimensioni estremamente ridotte. In studi precedenti dei autori, sono stati sviluppati approcci analitici per fornire una caratterizzazione acustica più completa del metamateriale proposto attraverso modelli di fluido equivalente. In questo lavoro, l'obiettivo è quello di far progredire il concetto introducendo la progettazione di un metamateriale acustico ventilato sub-lunghezza d'onda ed esaminandone la potenziale applicabilità in molteplici contesti edilizi, tra cui l'assorbimento acustico e il controllo della trasmissione del suono. Attraverso configurazioni geometriche ottimizzate, è possibile ottenere un assorbimento sonoro quasi perfetto (α > 0.8[-]) o un'efficienza superiore nella perdita di trasmissione sonora (> 30 [dB]) entro regimi sub-lunghezza d'onda. I risultati dimostrano che il metamateriale acustico proposto opera efficacemente a dimensioni ridotte e all'interno di bande di frequenza di attenuazione sintonizzate selettivamente, consentendo configurazioni a singola, doppia, tripla o esa-risonanza. Queste caratteristiche introducono ulteriori gradi di libertà nel concetto di design complessivo, offrendo applicazioni promettenti in vari settori dell'ingegneria, in particolare nell'acustica edilizia.
Parole chiave: materiale acustico, risonatori di Helmholtz, assorbimento sonoro, perdita di trasmissione sonora, acustica edilizia

1 | Introduction

In acoustics, the interest in manipulating the sound wave propagation on subwavelength regimes is a widely theorized field [1,2]. The development of acoustic metamaterials (AMMs) [3] has introduced new paradigms for the manipulation of sound wave propagation, leading to the exploration of novel non-natural physical behaviours.

Over the past two decades, AMMs have attracted considerable attention from the research community, as they offer a promising framework for the design of advanced noise mitiga-

[1] Vincitore ex-aequo del premio "Gino G. Sacerdote" edizione 2026.

tion strategies. This interest is largely driven by their lightweight nature, their effectiveness in the low-frequency regime, and their ability to exhibit broadband attenuation through engineered bandgap phenomena. Such characteristics enable effective noise control in the low- to mid-frequency range using compact, subwavelength configurations, making AMMs particularly well suited to engineering applications where space and weight constraints are critical, including building acoustics and ventilation systems [4].

The notorious interest in achieving these effective physical behaviours, characterized by the orderly and locally resonant response, inducing effective properties, i.e. single-negative acoustic metamaterials exhibiting effective bulk modulus [5], or effective negative density [6]; as well as double-negative or negative refractive index acoustic metamaterials [7], resulting from the resonance mechanism strictly dependent of the frequency.

Within this context, structures based on subwavelength resonant mechanisms represent a particularly promising solution for the development of compact and lightweight devices operating at low frequencies – typically below 1 kHz – where, for comparison, thin layers of conventional porous materials are generally ineffective [8]. A representative example is the Helmholtz resonator (HR), which offers significant potential for miniaturisation while inherently allowing passive airflow. Compared with traditional acoustic treatments, AMMs exhibit a high degree of design flexibility and tunability, enabling tailored control of acoustic responses. This adaptability, together with ongoing advances in manufacturing techniques, such as additive manufacturing, has enabled the fabrication of complex geometries at both micro- and macro-scales [9,10], thereby further broadening the applicability of such theoretical concepts and reinforcing their relevance for complex engineering solutions.

Among the emerging possibilities for sound wave manipulation, initially demonstrated by Fang *et al.* [11], acoustic metamaterials exhibiting an effective negative bulk modulus have repeatedly been shown to induce significant sound transmission loss. This behaviour is achieved by the compressive extensional phenomena induced by the airflow, related to the resonant effects in low-frequency regimes using subwavelength resonant elements, i.e. Helmholtz resonators [5,12]. Several studies have explored the induction of effective negative acoustic parameters and their implications for sound transmission control. In this context, Lee *et al.* [13] introduced a class of non-local resonator arrays consisting of periodically coupled ducts attached to a waveguide. Subsequently, Lan *et al.* [14] theoretically investigated nonlinear effects associated with sound propagation and dispersion in similar resonator array configurations. Recently, Jena *et al.* [15] examined multiple configurations of HRs arranged in parallel and series, observing the appearance of effective negative mass density and negative bulk modulus in finite arrays.

In contrast, other research efforts have focused on exploiting the distinctive acoustic properties of metamaterials and their strong miniaturization potential, enabling dimensions well below the acoustic wavelength. Representative examples include perfect absorption panels [16] and meta-diffusers [17], as well as extensions of these concepts toward the control of environmental noise. Such developments include meta-absorbers for façade acoustic insulation [18] and air-transparent acoustic insulation systems [19], all of which are fundamentally grounded in the classical theory of Helmholtz resonators.

Although acoustic metamaterials constitute a well-established and extensively theorized field within physics and engineering, recent years have seen a growing number of review studies addressing their potential applications in architectural and building acoustics. Arjunan *et al.* [20] identified a broad range of acoustic metamaterial concepts that can be adopted to improve the acoustic conditioning of buildings, highlighting their potentially transformative role in enhancing sound insulation performance in façades, ventilation systems, ducts, and window designs. Similarly, Rubino *et al.* [21] reported that research on acoustic metamaterials applied to noise insulation in architectural acoustics has yielded several promising concepts, demonstrated significant sound reduction capabilities, albeit often limited to narrow frequency bands. As noted by the authors, a major challenge remains the translation of these concepts into practical solutions, with a clear need for further investigations focused on full-scale implementations and real-world applications. Despite the encouraging attention received and the proliferation of small-scale and laboratory-based models, large-scale production and deployment remain limited, raising uncertainties regarding their economic feasibility and adoption within the construction industry.

Several studies have explored the theoretical concepts underlying acoustic metamaterials, a substantial gap remains in translating these advances into practical solutions capable of delivering optimised broadband noise attenuation and enhanced absorptive performance within the context of building acoustics. A significant portion of this gap can be attributed to manufacturing constraints and associated production costs, which become particularly critical when such systems are considered for large-scale civil engineering applications. These practical limitations often hinder their development and widespread implementation when compared with other engineering sectors, where fabrication tolerances and economic constraints may be less restrictive.

Accordingly, this stage of the research seeks to expand the novel design concept based on the parallel association of Helmholtz resonators by addressing its feasibility and functional relevance in realistic implementation scenarios, which had not been explored in earlier investigations. The present work proposes a multi-resonant modelling structure based on a compact panel composed of a matrix of resonant hexagonal sub-cells, which operates effectively at subwavelength dimensions and within selectively tuned attenuation frequency bands, enabling single-, dual-, triple-, or hexa-resonance configurations. By intentionally coupling the internal resonances of multiple resonant elements, the proposed structure enables an extended effective attenuation bandwidth, resulting in an optimized response to multiple acoustic problems within targeted frequency ranges.

This work is part of a PhD thesis conducted at the University of Coimbra (UC). The research was partly financed by FCT/MCTES through national funds (PIDDAC), under the R&D Unit Institute for Sustainability and Innovation in Structural Engineering (ISISE), within the scope of the project "*Study of passive ventilation devices with improved sound attenuation using metamaterials.*" It should be noted that the geometrical configuration and modelling framework adopted in this study build upon previous work by the authors, in [22], in which a theoretical approach was developed to assess the effective sound propagation properties of a parallel-sided branch inclusion of Helmholtz resonators under different termination conditions. The present study extends this framework by focusing on multi-resonator design strategies, the development of broadband and multi-functional configurations, and the exploration of potential building applications, including ventilated façade systems. Furthermore, this work incorporates experimental validation and optimisation procedures that were not addressed in the previous study.

The paper is organized as follows. Section 2 introduces the design concept of the proposed acoustic metamaterial. Section 3 presents the mathematical modelling and theoretical framework, together with its verification through finite element simulations, as well as the acoustic formulations employed in the analysis. Section 4 evaluates the acoustic performance of the system across multiple contexts, including sound absorption and sound transmission control. The analysis begins with an examination of the sound absorption characteristics and subsequently addresses the sound transmission loss performance. Although not the primary focus of the study, optimized configurations are also presented to highlight the acoustic capabilities of the proposed system for multiple applications. Section 5 discusses the multipurpose potential applications and inherent limitations, with particular emphasis on architectural integration, manufacturability, and scalability. Finally, Section 6 summarizes the findings by positioning the present work within the current state of the art and outlining potential directions for future developments and applications.

2 | Concept and geometrical design

Due to the inherent limitations of resonant systems, particularly their restricted effectiveness within narrow frequency bands, the concept of an in-parallel symmetric acoustic metamaterial is proposed, as illustrated in Figure 1. In this way, by proposing a hexagonal structure, being able to increase the number of holes and HRs per unit area, as well as to deal with greater area efficiency, when it is composed of a large number of cellular units.

More specifically, the proposed meta-structure consists of regular hexagonal units, composed by the in parallel association of 6 HRs, identical or not, in the same cross-section, with necks directed to the center of the hollow hole, as shown in Figure 1, so that the resonant effect of the cavities is activated by the sound waves that pass through each panel orifice.

Considering the classic model of the Helmholtz resonator, with the resonant frequency estimated from the equation, $f_\mathrm{r} = \frac{c_0}{2\pi}\sqrt{\frac{S}{(l_n + l_c)V}}$; where c_0 is the speed of sound in the air, V is the volume of the HR chamber, S is the neck opening area, l_n is the neck length, and l_c is the correction factor for a generic resonator.

The geometric description of the Helmholtz resonators is delineated in Figure 1, with the neck dimensions specified by, $l^{[n]}_{\mathrm{neck}}$ and $w^{[n]}_{\mathrm{neck}}$, representing the length and the width, respectively. The resonant cavity volume, $V^{[n]}_{\mathrm{cav}}$, is computed from $l^{[n]}_{\mathrm{cav}}$ and $w^{[n]}_{\mathrm{cav}}$, denoting the length and width of the cavity, respectively. Highlighting that the superscript $[n]$ corresponds to the order of the included resonator.

Concerning the complex geometrical configuration, three propositions will be presented: the single, dual, and triple, and hexa configurations. These are defined by the number of group sets and the number of local resonances within each configuration, which will be better explained in the next sections.

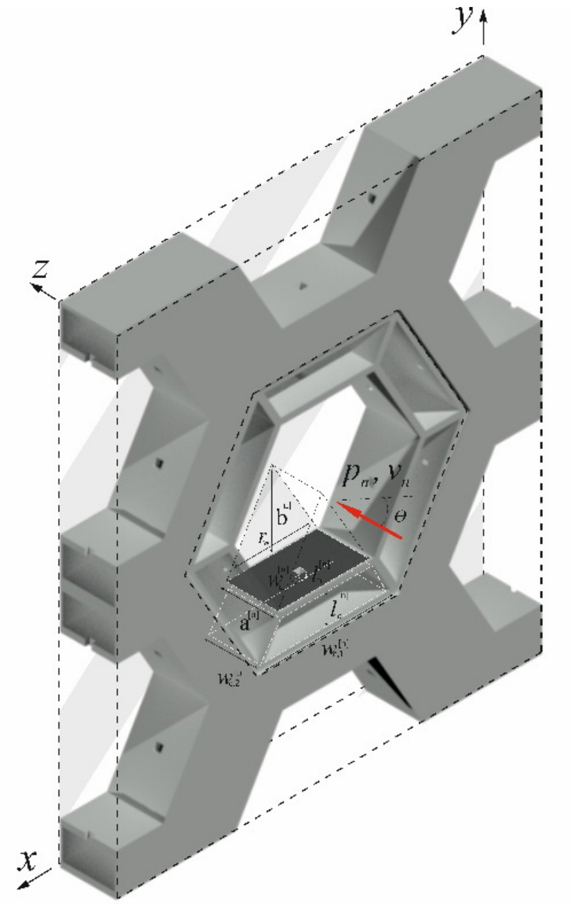

Fig. 1 – Illustrative diagram of hexagonal acoustic metamaterial panel
Diagramma illustrativo del pannello metamateriale acustico esagonale

Following the recent trends of using additive manufacturing techniques in the context of prototyping acoustic metamaterials, the proposed acoustic metamaterials under analysis were modelled in a dedicated 3D Computer-Aided Design (CAD) and manufactured at the *Institute for Sustainability and*

Innovation in Structural Engineering – ISISE in the Civil Engineering Department at the University of Coimbra, Portugal.

As photographed in Figure 2, the materialized acoustic hexagonal metamaterial using a fused-deposition modelling (FDM) technique. The additive manufacturing technique employed consists of deposition of polylactic acid filaments (PLA), through a nozzle extruder of 0.4 mm of diameter, as seen in Fig. 2 (a), using a 3D printer Blocks One MK2. Tab. 1 summarizes the information regarding the manufacturing settings employed.

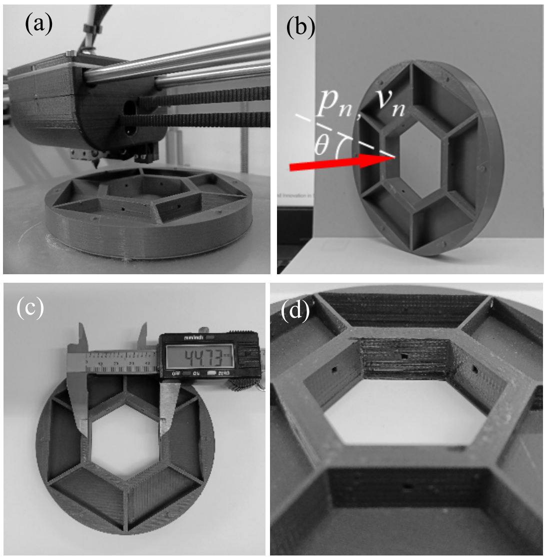

Fig. 2 – Design and manufacturing of acoustic hexagonal metamaterial. (a) Photography of the printing machine in operation. (b) – (d) Samples of the multi-resonant metamaterial structure with the respective dimension in millimetres (mm).

Progettazione e produzione di metamateriale acustico esagonale. (a) Fotografia della macchina da stampa in funzione. (b) – (d) Campioni della struttura del metamateriale multirisonante con le rispettive dimensioni in millimetri (mm)

Tab. 1 – Summary of the 3D printing device, material, and manufacturing parameters

Caratteristiche di fabbricazione del dispositivo di stampa 3D

Features		*Definitions*
Device characteristics	Device	Blocks One MK2
	Technology	Fused filament fabrication
	Max built volume-	200 x 210 x 210 mm³
	Nozzle diameter	0.4 mm
	Slicing software	Ultimaker Cura v. 4.9.0
Material characteristics	Material	Polytactic acid
	Filament diameter	1.75mm
Manufacturing settings	Layer resolution	0.1 mm
	Line width	0.4 mm
	Infill density	25%
	Printing Temperature	210°C
	Build Plate Temperature	50°C
	Print Speed	50 mm s-1

3 | Mathematical modelling

3.1 | Analytical framework

3.1.1 | Viscous thermal losses and Transfer Matrix Method

To describe the sound waves propagation in the acoustic metamaterial panel, the analytical prediction model is developed based on the transfer matrix method and equivalent fluid approach adapted from [23,24], where from the equivalent medium theory each region can be homogenized as function of equivalent density $\rho_{\mathrm{eff}}^{[n]}$ and equivalent bulk modulus $K_{\mathrm{eff}}^{[n]}$, described as follows:

$$\rho_{eff}(\omega) = \rho_0\alpha_\infty\left(1+\frac{\phi\sigma}{j\omega\rho_0\alpha_\infty}\left(1+j\frac{4\omega\rho_0\eta\alpha_\infty^2}{\sigma^2\phi^2\Lambda^2}\right)^{\frac{1}{2}}\right), \quad (1)$$

$$K_{eff}(\omega) = \frac{\gamma P_0}{\gamma-(\gamma-1)\left(1+\frac{8\eta}{j\omega Pr\rho_0\Lambda'^2}\left(1+j\frac{\omega Pr\rho_0\Lambda'^2}{16\eta}\right)^{\frac{1}{2}}\right)^{-1}}, \quad (2)$$

in general, assuming narrow orifices, the thermal and viscous characteristic lengths, $\Lambda = \Lambda'$, are numerically equal to the hole's hydraulic radius $r_{\mathrm{i}}^{[n]} = w_{\mathrm{i}}^{[n]}/\sqrt{\pi}$ (here, the subscript i, is related to the i-th generical part of the system); and the respective values $\gamma = 1.4$ being the specific heat ratio, Pr is the Prandtl number, $\rho 0 = 1.23$ kg/m³ is the mass density, $\eta = 1.82\times10{-}5$ Pa·s is the air dynamic viscosity, and $P0 = 101325$ Pa is the static pressure, defines the thermodynamic properties of air saturating the system.

As previously discussed in Refs. [22] the analytical estimations of the transport parameters describe the resistive part induced by the viscous effects inside the hole, as well the flux distortion in the acoustic field in the front rigid layers. Tab. 2 lists the reliable analytical transport parameters expressions, for the Johnson Champoux Allard (JCA) rigid frame model.

Tab. 2 – Analytical estimations of the transport parameters

Stime analitiche dei parametri di trasporto

σ	Specific airflow resistivity	$\left(\frac{2\,l_{\mathrm{neck}}^{[n]}}{r_{\mathrm{neck}}^{[n]}}+4\right)\frac{R_s}{\phi}\frac{1}{l_{\mathrm{neck}}^{[n]}}$	*Pa · s/m²*
ϕ	Open porosity	1	[–]
R_s	Surface resistive term	$\frac{\sqrt{2\eta\omega\rho_0}}{2}$	*Pa · s/m*
α_∞	Geometric tortuosity	$1+\frac{2\,\varepsilon_c}{l_{\mathrm{neck}}^{[n]}}$	[–]
ε_c	Length correction	$\varepsilon_c = 0.85 r_{\mathrm{neck}}^{[n]}\,F(\varepsilon)$	[–]

Consequently, for analytical considerations, the transfer matrix method (TMM) is used to describe the acoustic plane wave propagation in an acoustic symmetric system, as illustrated in Fig. 3.

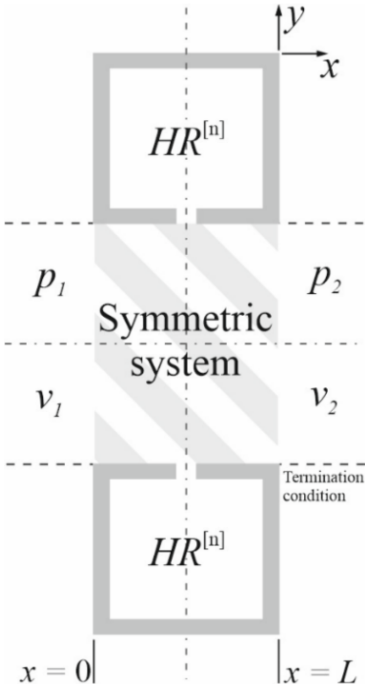

Fig. 3 – Schematic diagram of the TMM approach applied to the acoustic metamaterial symmetric system problem. Figure re-plicated from [22]

Diagramma schematico dell'approccio TMM applicato al problema del sistema simmetrico di metamateriali acustici. Figura riprodotta da [22]

Given the continuity condition between the incident sound pressure and particle velocity from an initial position, p_1 and v_1, respectively, to the final position, p_2 and v_2, with the assembly of matrix elements being written by:

$$\mathbf{T}\begin{bmatrix} p_1 \\ v_1 \end{bmatrix}_{x=0} = \mathbf{T}_{\mathrm{w}}^{[n]}\mathbf{T}_{\mathrm{HR}}^{[1]}\cdots\mathbf{T}_{\mathrm{HR}}^{[n-1]}\mathbf{T}_{\mathrm{HR}}^{[n]}\mathbf{T}_{\mathrm{w}}^{[n]} = \mathbf{T}\begin{bmatrix} p_2 \\ v_2 \end{bmatrix}_{x=\mathrm{L}}. \tag{3}$$

Here, the sound wave radiation for an arbitrary segment part of the system, herein represented by $\mathbf{T}_{\mathrm{i}}^{[n]}$, is expressed by the transfer matrix [23,24]:

$$\mathbf{T}_{\mathrm{i}}^{[n]} = \begin{bmatrix} \cos\left(k_{\mathrm{i}}^{[n]} l_i\right) & \mathrm{j}Z_i^{[n]}\sin\left(k_i^{[n]} l_i\right) \\ \mathrm{j}\sin\left(k_i^{[n]} l_i\right)/Z_i^{[n]} & \cos\left(k_i^{[n]} l_i\right) \end{bmatrix}, \tag{4}$$

where $k_{\mathrm{i}}^{[n]}$ and l_i, are, respectively, the wavenumber and length of the waveguide, and $Z_{\mathrm{i}}^{[n]}$ is the characteristic impedance of the waveguide.

3.1.2 | *Sound absorption descriptors based on the transfer matrix terms*

Considering an absorptive behavior of the acoustic system the following rigidly backed termination condition is imposed under analysis. In order to neglect the transmitted longitudinal waves through the system, and assuming the total transfer matrix T (Eq. 3) for the previously described acoustic system, the reflection coefficient is given by [22]:

$$R_{\mathrm{p}} = \frac{T_{11} - T_{21}\,\rho_0 c_0}{T_{11} + T_{21}\,\rho_0 c_0}. \tag{5}$$

The corresponding sound absorption coefficient under normal incidence conditions, is defined as:

$$\alpha = 1 - \left|R_{\mathrm{p}}\right|^2. \tag{6}$$

3.1.3 | *Sound transmission descriptors based on the transfer matrix terms*

In case of a transmission problem, the complex transmission coefficient T_p, defined as the ratio between transmitted and incident wave amplitudes. Thus, assuming the symmetry and reciprocity of the acoustic system, the transmission coefficient can be written as [22]:

$$T_{\mathrm{p}} = \frac{2\mathrm{e}^{\mathrm{j}kL}}{T_{11} + T_{12}/Z_0 + Z_0 T_{21} + T_{22}}; \tag{7}$$

Finally, the sound transmission loss (TL) in decibel is:

$$\mathrm{TL} = 20\log_{10}\left(\frac{1}{|T_{\mathrm{p}}|}\right). \tag{8}$$

3.2 | Experimental and numerical verification

To validate the proposed theoretical model, the acoustic metamaterials were investigated through both numerical simulations and experimental measurements. The experimental campaign was partially carried out at the Acoustic Research Group of the Engineering Department of the University of Ferrara.

The normal-incidence sound absorption and reflection coefficients under finite sample conditions were measured using the two-microphone transfer function method, in accordance with ISO 10534-2 [25]. In brief, the experimental setup consisted of a cylindrical impedance tube with an inner diameter of d = 45 mm, operating over a frequency range from 50 Hz to 4150 Hz. During testing, the samples were mounted inside the tube and backed by a rigid termination. A sine-sweep excitation was generated by a loudspeaker positioned at the upstream end of the tube. The acoustic pressure was measured at two distinct locations, p_1 and p_2, corresponding to axial positions x_1 and x_2, respectively. These measurements were used to compute the transfer function H_{12}, enabling the decomposition of the sound field into incident and reflected wave components. This procedure allowed the determination of the normal-incidence sound absorption coefficient. It should be noted that the experimental campaign in the present study was restricted to the characterization of sound absorption. The sound transmission loss was instead assessed through analytical modelling and finite element simulations, following the ASTM E2611 [26] framework. Within this approach, the transfer matrix components, as defined in Eq. 3, can be systematically obtained.

To evaluate the accuracy of the proposed model, the results were compared with experimental measurements and numerical simulations performed using the finite element method (FEM) in COMSOL Multiphysics. Numerical simulations were conducted under plane wave propagations conditions. Rigi boundary conditions were imposed on the lateral walls to enforce zero normal particle velocity. At the excitation side, a prescribed acoustic pressure was applied to generate the incident wave. To ensure the acoustic response under two different termination conditions. For sound absorption measurements, the model replicated ISO 10534-2 [25] employing a rigid termination. For normal-incidence sound transmission, the model followed ASTM E2611-09 [26], where a Perfect Matched Layer (PML) was applied at the termination to simulate an anechoic boundary condition. This configuration maintains consistency with the assumptions employed in both the analytical model and the experimental setup.

Assuming a time-harmonic dependence of the form $e^{i\omega t}$, the simulations were conducted in the pressure acoustics domain. The main acoustic domain, corresponding to the air-filled impedance tube, was discretized using tetrahedral elements with a maximum element size equal to $\lambda_{\text{min}}/8$, where $\lambda_{\text{min}} = c_0/f_{\text{max}}$. This criterion ensures at least eight elements per wavelength throughout the computational domain. To accurately model viscous and thermal losses in critical regions the Thermoviscous Acoustics Module in COMSOL Multiphysics was employed. For the mesh discretization in narrow regions, such as resonator necks, a refined mesh was employed. In these regions, the maximum element size was limited to $w_{\text{neck}}^{[n]}/4$, while the minimum element size was set to $\delta_V/2$, where $\delta_V = \sqrt{2\mu/(\rho_0\omega)}$ represents the viscous boundary layer thickness.

Inside the resonator cavities, where dissipative effects are less significant, the maximum element size was set to $w_{\text{cav}}^{[n]}/2$ and the minimum to $w_{\text{cav}}^{[n]}/4$. In the remaining parts of the domain, a multi-size mesh strategy was used to balance accuracy and computational efficiency. All external boundaries of the acoustic domain were assumed to be perfectly rigid. After defining the governing equations, excitation, and boundary conditions, a linear system was solved in the frequency domain using a direct solver for each frequency step between 100 Hz and f_{max}.

Table 3 summarizes the mesh size criteria adopted for each region of the computational domain within the Thermoviscous Acoustics Module.

Tab. 3 – Summary of the mesh size criteria adopted for each region of the computational domain within the Thermoviscous Acoustics Module in COMSOL software

Riepilogo dei criteri di dimensione della maglia adottati per ciascuna regione del dominio computazionale all'interno del modulo di acustica termoviscosa in COMSOL Software

Domain region	*Maximum element size*	*Minimum element size*
Neck region	$w_{\text{neck}}^{[n]}/4$	$\delta_V/2$
Waveguide region	$r_{\text{wave}}^{[n]}/4$	$\delta_V/2$
Cavity region	$w_{\text{cav}}^{[n]}/2$	$w_{\text{cav}}^{[n]}/4$
Boundary layer zones	Adaptive (local refinement)	$\delta_V/2$
Remaining acoustic domain	$\lambda_{\text{min}}/8$	Automatic (multi-size)

4 | Acoustic Performance Assessment

To illustrate the versatility of the developed design, the following subsections present both the absorption and sound transmission performances of the proposed system. Although algorithmic optimisation does not constitute the primary focus of the present study, these were nonetheless employed in the geometric definition of the configurations examined herein. Thus, to facilitate a clearer interpretation of the results presented subsequently, a concise overview of the adopted optimisation framework is first provided. This description aims to contextualise the geometric tuning procedure and to clarify the rationale underlying the selected design configurations.

4.1 | Illustrative example of optimised sound absorption for the proposed AMM

Given the intrinsic complexity associated with establishing optimal conditions for sound absorption, illustrative examples of the absorptive performance of the proposed acoustic metamaterial are presented herein. The objective is to demonstrate representative configurations capable of achieving enhanced absorption within prescribed target frequency ranges, evidencing how the design proposition can be expanded for multipurpose acoustic scenarios.

As widely established in the theoretical framework of resonant absorbers, perfect sound absorption can be achieved under the critical coupling condition, in which the external radiation leakage is precisely balanced by the intrinsic visco-thermal dissipation mechanisms of the system. Under this condition, surface impedance matching between and the surrounding medium is satisfied. Mathematically, this requires that, at the target resonance frequency, the real part of the effective surface impedance equals the characteristic impedance of air $\text{Re}(Z_{eff}) = Z_0$, while the imaginary part vanishes $\text{Im}(Z_{eff}) = 0$. When these conditions are fulfilled, reflection is suppressed and the incident acoustic energy is entirely dissipated within the structure [27].

Based on the analytical formulations implemented in the present work, a Sequential Quadratic Programming (SQP) procedure was employed in conjunction with the Transfer Matrix Method (TMM) to determine optimised geometric parameters. This optimisation framework enables the systematic identification of resonator dimensions capable of inducing perfect or near-perfect absorption, consistent with the critical coupling mechanism previously reported in [27].

By enforcing the coupling condition previously described, the objective function is formulated to maximise the sound absorption coefficient at the prescribed target frequency, such that $|\alpha_{\text{HR},i}(f_{\text{target},i})| = 1$ More explicitly, the nonlinear optimisation problem is expressed in the following form,

$$\begin{aligned} &\text{minimize } \mathcal{F}(x) = -\sum_{i=1}^{n} \left|1 - \alpha_{HR,i}\right|, \\ &\text{Subject to } b_l \leq \begin{bmatrix} f_{\text{target},i} \\ w_{neck}^{[n]} \\ V_{cav}^{[n]} \end{bmatrix} \leq b_u. \end{aligned} \tag{9}$$

As initial elucidation, Figure 4 corresponds to the first design proposal, which achieves a single local resonance frequency at f_{single} = 550 H. Table 4 summarizes the optimal geometrical parameters.

Tab. 4 – Geometrical parameters of the single-resonance configuration, optimisation bounds and corresponding optimized geometric parameters (all dimensions in millimetres)

Parametri geometrici della configurazione a risonanza singola, limiti di ottimizzazione e corrispondenti parametri geometrici ottimizzati (tutte le dimensioni sono in millimetri)

	$f_{\text{target},}i$ [Hz] *Optimized Value*	$w^{[n]}_{\text{neck}}$[mm] *Optimized Value*	$l^{[n]}_{\text{neck}}$ [mm] *Nominal Value*	$V^{[n]}_{\text{cav}}$ [mm³] *Optimized Value*
f_{single}	550	2.40	5.00	7.34×10³

As demonstrated, in Figure 4, the system reached perfect sound absorption under normal incidence. It is further observed that the proposed optimisation framework effectively preserves the critical loss balance by modulating viscothermal dissipation through the coordinated operation of the six resonators, thereby enabling the achievement of the critical coupling condition. A detailed discussion of the relationship between critical coupling condition and the acoustic performance of the hexagonal acoustic metamaterial can be found in [28].

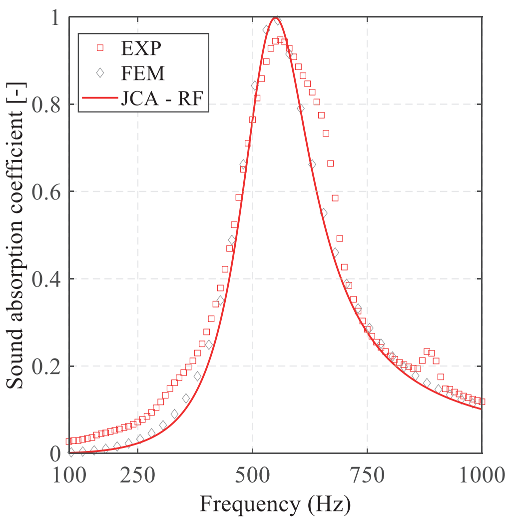

Fig. 4 – Comparison of the sound absorption coefficient spectra for single resonance model determined with the analytical JCA equivalent-fluid approach using TMM (solid red line), using finite element method (grey markers) and experimentally measured (square red markers)

Confronto degli spettri del coefficiente di assorbimento acustico per il modello a risonanza singola determinati con l'approccio analitico del fluido equivalente JCA utilizzando TMM (linea rossa continua), utilizzando il metodo degli elementi finiti (marcatori grigi) e misurati sperimentalmente (marcatori rossi quadrati)

A slight deviation observed within the frequency range of interest in the experimental results may be attributed to minor inaccuracies inherent to the 3D printing process. As reported in [9,29], small variations in printing resolution can lead to shifts in the resonant frequency range. This effect is also evident in the present models, given the resolution limits of the employed manufacturing techniques and the strong geometric sensitivity associated with achieving critical coupling between closely spaced resonances. In such systems, the resonant behaviour is directly governed by the geometric dimensions of the structure.

To demonstrate the effect of critical coupling in achieving broadband perfect absorption, a preliminary multi-resonant concept involving multiple local resonance frequencies is presented.

As initial example, the dual resonance proposition is composed of two sets of three resonators each, tuned into two different frequencies acting together in parallel circumstances. Figure 5 shows the dual resonance proposition, with resonance frequencies set at $f^{[1]}_{\text{dual}}$ = 560 Hz and $f^{[2]}_{\text{dual}}$ = 625 Hz. The corresponding optimised geometric parameters are summarised in Table 5.

Tab. 5 – Geometrical parameters of the dual-resonance configuration, optimisation bounds and corresponding optimized geometric parameters. (all dimensions in millimetres)

Parametri geometrici della configurazione a doppia risonanza, limiti di ottimizzazione e corrispondenti parametri geometrici ottimizzati. (tutte le dimensioni sono in millimetri)

	$f_{\text{target},}i$ [Hz] *Optimized Value*	$w^{[n]}_{\text{neck}}$[mm] *Optimized Value*	$l^{[n]}_{\text{neck}}$ [mm] *Nominal Value*	$V^{[n]}_{\text{cav}}$ [mm³] *Optimized Value*
$f^{[1]}_{\text{dual}}$	560	2.15	5.0	5.30×10³
$f^{[2]}_{\text{dual}}$	625	2.15	5.0	4.28×10³

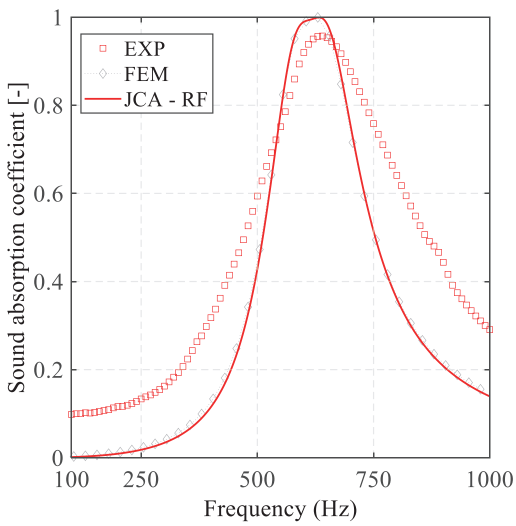

Fig. 5 – Comparison of the sound absorption coefficient spectra for dual resonance model determined with the analytical JCA equivalent-fluid approach using TMM (solid red line), using finite element method (grey markers) and experimentally measured (square red markers)

Confronto degli spettri del coefficiente di assorbimento acustico per il modello a doppia risonanza determinato con l'approccio analitico del fluido equivalente JCA utilizzando TMM (linea rossa continua), utilizzando il metodo degli elementi finiti (marcatori grigi) e misurato sperimentalmente (marcatori rossi quadrati)

Figure 5 indicates that the dual proposition establishes a strong coupling condition between the near local resonances, resulting in an effective absorption bandwidth of approximately Δf = 100 Hz. Within this interval, near perfect and perfect absorption levels are achieved, with $\alpha > 0.8$, as illustrated by the red solid line.

In the triple-resonance scenario, the results presented in Figure 6 correspond to a configuration comprising three distinct resonators tuned to $f^{[1]}_{tripe}$ = 570 Hz, $f^{[2]}_{tripe}$ = 620 Hz, and $f^{[3]}_{tripe}$ = 740 Hz, each consisting of pairs of symmetrically positioned resonators. The optimized geometric parameters are provided in Table 6.

Tab. 6 – Geometrical parameters of the triple-resonance configuration, optimisation bounds and corresponding optimized geometric parameters (all dimensions in millimetres)

Parametri geometrici della configurazione a tripla risonanza, limiti di ottimizzazione e corrispondenti parametri geometrici ottimizzati (tutte le dimensioni sono in millimetri)

	$f_{target,i}$ [Hz]	$w^{[n]}_{neck}$ [mm]	$l^{[n]}_{neck}$ [mm]	$V^{[n]}_{cav}$ [mm³]
	Optimized Value	*Optimized Value*	*Nominal Value*	*Optimized Value*
$f^{[1]}_{tripe}$	570	2.5	5.0	7.3×10³
$f^{[2]}_{tripe}$	620	2.35	5.0	5.5×10³
$f^{[3]}_{tripe}$	740	2.5	5.0	4.2×10³

The normal-incidence sound absorption coefficient for the triple-resonance model, obtained analytically and numerically, and subsequently validated through experimental measurements. The optimised configuration achieves perfect absorption at the target frequencies and provides an effective absorption bandwidth of approximately Δf = 220 Hz for absorption levels exceeding $\alpha > 0.8$.

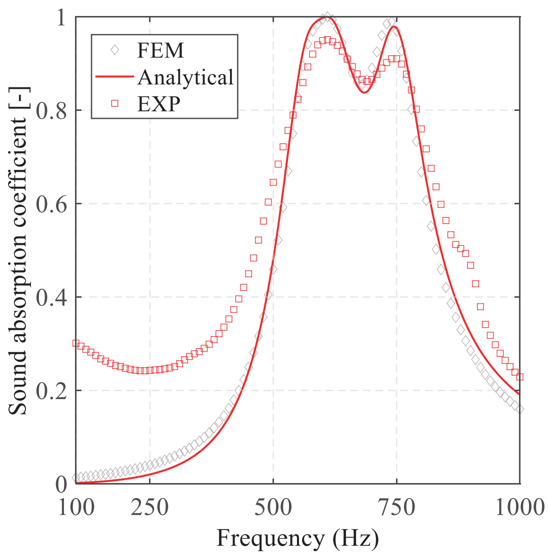

Fig. 6 – Comparison of the sound absorption coefficient spectra for triple resonant model determined from the analytical JCA fluid-equivalent approach using TMM (solid red line), using finite element method (grey markers) and measured experimentally (square red markers)

Confronto degli spettri del coefficiente di assorbimento acustico per il modello triplo risonante determinato dall'approccio fluido-equivalente JCA analitico utilizzando TMM (linea rossa continua), utilizzando il metodo degli elementi finiti (marcatori grigi) e misurato sperimentalmente (marcatori rossi quadrati)

To provide an attempt towards broadband sound absorption, a more complex acoustic metamaterial (AMM) configuration is now proposed. In this advanced scenario, the geometric parameters required to achieve perfect absorption in each individual Helmholtz resonator of the proposed AMM.

The broadband configuration presented in Figure 7 is obtained through the progressive incorporation of multiple Helmholtz resonators within the unit cell from n = 1, 2, 3, ... 6. In this circumstance, the frequency range is manually defined, with $f_{target,i}$ = [300 Hz, 700 Hz]. The proposed optimisation procedure enforces the critical coupling condition between adjacent local resonances, resulting in an effective bandwidth of approximately Δf = 300 Hz. Within this interval, the absorption valleys between neighbouring resonances are significantly reduced, approaching near-perfect absorption $\alpha > 0.8$. The corresponding dimensions for each configuration are reported in Table 7, ensuring full reproducibility of the proposed design.

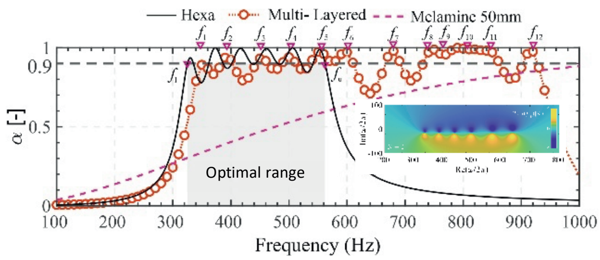

Fig. 7 – Sound absorption spectra of Optimized Hexagonal configuration at normal incidence. The black solid line indicates the analytical values for the sound absorption coefficient. The red line with markers represents a multi-layered acoustic meta structure. The dashed pink line illustrated a sound absorption spectrum of a melamine layer of 50mm thickness. The detailed image represents the complex frequency evidencing the coupling condition

Spettri di assorbimento acustico della configurazione esagonale ottimizzata a incidenza normale. La linea nera continua indica i valori analitici del coefficiente di assorbimento acustico. La linea rossa con i marcatori rappresenta una metastruttura acustica multistrato. La linea tratteggiata rosa illustra lo spettro di as-sorbimento acustico di uno strato di melammina di 50 mm di spessore. L'immagine dettagliata rappresenta la frequenza complessa che evidenzia la condizione di accoppiamento.

The coloured contour plot further depicts the complex frequency plane representation of the poles (yellow markers) and zeros (blue markers) of the reflection coefficient, expressed as log |R²|, thereby evidencing the evolution of the critical coupling mechanism in the proposed design. As a brief explanation, in the complex frequency plane, the eigenvalue R is associated with the scattering matrix, and its corresponding poles and zeros govern the reflection characteristics along the real frequency axis. Each zero-pole pair corresponds to a resonant mode of the system. In the critically coupled condition, zero (represented by circular markers) lies on the real frequency axis. The presence of a zero on the real axis therefore satisfies the critical coupling condition and corresponds to perfect sound absorption. For a more comprehensive explanation see [28].

For comparison, when analysing a conventional 50 mm thick melamine foam layer, dashed pink line, it is observed that the proposed thinner metamaterial configuration exhibits superior performance in the low-frequency range. Achieving a comparable level of low-frequency attenuation using traditional porous materials would typically require a substantial increase in thickness.

Tab. 7 – Geometrical parameters of the hexa-resonance configuration, optimized geometric parameters (all dimensions in millimetres)

Parametri geometrici della configurazione a risonanza esagonale, parametri geometrici ottimizzati (tutte le dimensioni sono in millimetri)

$f_{\text{target},i}$ [Hz]	$w^{[n]}_{\text{neck}}$ [mm]	$l^{[n]}_{\text{neck}}$ [mm]	$V^{[n]}_{\text{cav}}$ [mm^3]
340	1.45	5.0	7.0×10^3
385	1.50	5.0	5.6×10^3
440	1.52	5.0	4.5×10^3
500	1.64	5.0	4.0×10^3
565	1.91	5.0	4.0×10^3
630	2.20	5.0	4.0×10^3

In summary, the association of Helmholtz resonators (HRs) within the waveguide enables the controlled interaction of multiple local resonances, facilitating the achievement of perfect or quasi-perfect absorption. In the present configuration, up to six absorption peaks are obtained under near critical and critical coupling conditions. As the number of local resonances increases, the effective absorption bandwidth is progressively widened without compromising the loss balance. This behaviour is associated with an increased number of poles-zero pairs in the complex frequency plane, ensuring the presence of zeros on the real frequency axis and, consequently, observable perfect absorption.

4.2 | Illustrative examples of optimised sound Transmission loss capacity of the proposed AMM

In this subsection, the sound transmission capacity of the proposed acoustic metamaterial is analysed. A geometrical optimization is performed from the Sequential Quadratic Programming (SQP) grounded in the analytical formulations, to determine the set of resonator parameters $\left\{w^{[n]}_{neck}, l^{[n]}_{neck}, V^{[n]}_{cav}\right\}$, for the proposed, single, dual, triple case, in order to maximize the STL at a predetermined local resonant frequency $f_{\text{target},i}$. The problem is explicitly defined as follows,

$$\text{minimize } \mathcal{F}(x) = -\sum_{i=1}^{n} \text{STL}\left(x, f_{\text{target},i}\right),$$
$$\text{Subject to } b_l \leq \begin{bmatrix} w^{[n]}_{neck} \\ l^{[n]}_{neck} \\ V^{[Mn]}_{cav} \end{bmatrix} \leq b_u, \tag{10}$$

where, the objective function $\mathcal{F}(x)$ seeks to determine the geometric parameters design x within the upper and lower bounds, b_l and b_u, at the i-th target frequencies.

For the first case, in a single resonance frequency, f_{single} = 935 Hz, the optimized sound transmission loss (STL) can be evidenced. Table 8 summarizes the optimized geometrical parameters. For further details regarding the selection of the bound limits, the reader is referred to [28].

Tab. 8 – Geometrical parameters of the single-resonance configuration, optimized geometric parameters (all dimensions in millimetres)

Parametri geometrici della configurazione a risonanza singola, parametri geometrici ottimizzati (tutte le dimensioni sono in millimetri)

$f_{\text{target},i}$ [Hz]	$w^{[n]}_{\text{neck}}$ [mm]		$l^{[n]}_{\text{neck}}$ [mm]		$V^{[n]}_{\text{cav}}$ [mm^3]	
	Nominal Value	*Optimized Value*	*Nominal Value*	*Optimized Value*	*Nominal Value*	*Optimized Value*
935	2.5	4.3	2.5	2.5	4.62 ×10^3	1×10^4

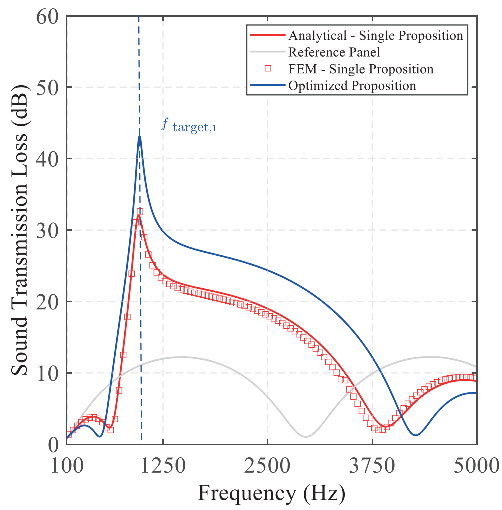

Fig. 8 – Sound transmission loss of the compact single-resonant panel configuration under normal incidence. Square markers denote the numerical results, while the red curves correspond to the analytical predictions for the proposed single acoustic metamaterial (AMM). The grey curve represents the reference STL values, and the blue curves indicate the optimized response

Perdita di trasmissione sonora della configurazione compatta a pannello singolo risonante in incidenza normale. I marcatori quadrati indicano i risultati numerici, mentre le curve rosse corrispondono alle previsioni analitiche per il metamateriale acustico singolo (AMM) proposto. La curva grigia rappresenta i valori STL di riferimento e le curve blu indicano la risposta ottimizzata

Figure 8 shows a localized enhancement at the specified resonant frequency, f_{single} = 935 Hz, where the STL value reaches approximately 35 dB. This enhancement, attributed to the locally resonant inclusion, amplifies the inherent attenuation caused by the waveguide constriction, characterized by ϕr < 1, as observed in the grey solid line. The solid lines in Figure 8 represent the results from the proposed analytical model, which incorporates losses throughout the system. From the initial optimization scenario, the blue line exhibits the optimal sound transmission loss curve at the target frequency a pronounced peak with an enhancement of approximately 10 dB relative to the reference configuration (depicted by the red curve). Thereby validating the effectiveness of the optimisation strategy in improving attenuation at the prescribed resonance frequency.

By extending the objective function, defined in Equation 10, to include additional resonance frequencies ($f_{target,2}$ and $f_{target,3}$). In this scenario, Figure 9 illustrates the optimized sound transmission loss for a dual resonance configuration, showing the interaction of two near-resonant frequencies, $f^{[1]}_{dual}$ = 935 Hz and $f^{[2]}_{dual}$ = 1095 Hz, where the STL values reach magnitudes of 28 dB and 34 dB, respectively. Table 9 summarizes the optimised geometric parameters for the proposed configuration. Figure 9 shows that the optimised configuration (blue curve) achieves an STL increase of approximately 5 dB at each resonance frequency, confirming the effectiveness of the dual-resonance design.

Tab. 9 – Geometrical parameters of the dual-resonance configuration, optimisation bounds and corresponding optimized geometric parameters (all dimensions in millimetres)

Parametri geometrici della configurazione a doppia risonanza, limiti di ottimizzazione e corrispondenti parametri geometrici ottimizzati (tutte le dimensioni sono in millimetri)

$f_{target,i}$ [Hz]	$w^{[n]}_{neck}$ [mm]		$l^{[n]}_{neck}$ [mm]	$V^{[n]}_{cav}$ [mm³]	
	Nominal Value	*Optimized Value*	*Nominal Value*	*Nominal Value*	*Optimized Value*
f_{single}	2.5	4.3	2.5	4.62 ×10³	1×10⁴
$f^{[2]}_{dual}$	3.0	4.9			

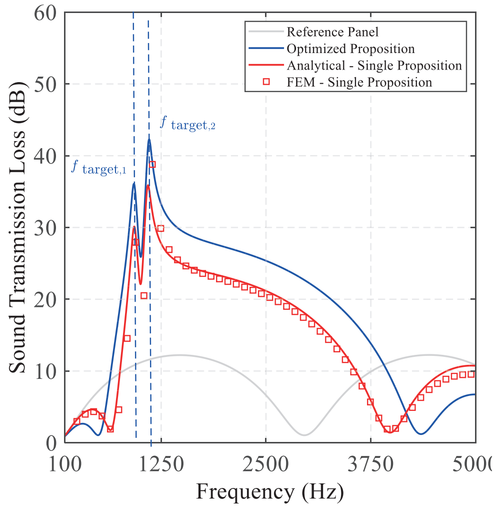

Fig. 9 – Sound transmission loss of the compact dual resonant panel configuration at normal incidence. The square markers indicate the numerical verification, and the red curves represent the analytical prediction for the proposed dual resonance proposition. The grey curve represents the reference STL values, and the blue curves indicate the optimized response

Perdita di trasmissione sonora della configurazione compatta a doppio pannello risonante ad incidenza normale. I marcatori quadrati indicano la verifica numerica, mentre le curve rosse rappresentano la previsione analitica per la proposta di doppia risonan-za. La curva grigia rappresenta i valori STL di riferimento, e le curve blu indicano la risposta ottimizzata

Finally, Figure 10 illustrates the triple resonance scenario, involving the parallel symmetric association of three distinct local resonances. In this configuration, the width of the first resonator neck, $w^{[1]}_{neck,triple}$ = 2.5 mm, the second $w^{[2]}_{neck,triple}$ $w^{[1]}_{neck,triple}$ = 3.0 mm, and the third $w^{[3]}_{neck,triple}$ = 4.0 mm, are varied, while maintaining the remaining geometric parameters. These variations induce resonance frequencies of $w^{[1]}_{triple}$ = 935 Hz, $w^{[2]}_{triple}$ = 1095 Hz, and $w^{[3]}_{triple}$ = 1390 Hz, respectively. Table 10 summarizes the triple-resonances geometric configuration.

Tab. 10 – Geometrical parameters of the triple-resonance configuration, optimisation bounds and corresponding optimized geometric parameters. (all dimensions in millimetres)

Parametri geometrici della configurazione a tripla risonanza, limiti di ottimizzazione e corrispondenti parametri geometrici ottimizzati (tutte le dimensioni sono in millimetri)

$f_{target,i}$ [Hz]	$w^{[n]}_{neck}$ [mm]		$l^{[n]}_{neck}$ [mm]		$V^{[n]}_{cav}$ [mm³]	
	Nominal Value	*Optimized Value*	*Nominal Value*	*Optimized Value*	*Nominal Value*	*Optimized Value*
$f^{[1]}_{triple}$	2.5	4.30		2.50		
$f^{[2]}_{triple}$	3.0	4.90	2.5		4.62 ×10³	1×10⁴
$f^{[3]}_{triple}$	4.0	8.80		7.50		

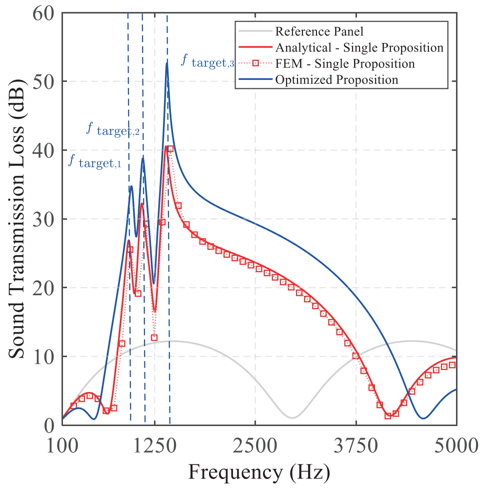

Fig. 10 – Sound transmission loss of the compact triple resonant panel configuration at normal incidence. The square markers indicate the numerical verification, and the red curves represent the analytical prediction for the proposed AMM. The grey curve represents the reference STL values, and the blue curves indicate the optimised response

Perdita di trasmissione sonora della configurazione compatta a triplo pannello risonante ad incidenza normale. I marcatori quadrati indicano la verifica numerica, mentre le curve rosse rappresentano la previsione analitica per il modello analitico proposto. La curva grigia rappresenta i valori di riferimento di perdita di trasmissione sonora (STL), e le curve blu indicano la risposta ottimizzata

In Figure 10, peak amplitudes of 25 dB, 30 dB, and 38 dB are observed, corresponding to the first, second, and third resonance frequencies, respectively. In a optimized context, upon the introduction of a third target frequency, the blue curve exhibits an additional sound transmission loss (STL) enhancement exceeding 5 dB at the third resonance, thereby contributing to a further broadening of the effective attenuation bandwidth.

As a preliminary result, Figure 11 presents the predicted sound transmission loss (STL) of the proposed metamaterial, considering a prescribed target frequency range of [fL, fU] = [800, 1600] Hz defined during the optimisation process. A minimum attenuation gap of ΔTLtarget = 5 dB and a minimum frequency spacing of Δfmin = 200 Hz were imposed as strict constraints to ensure adequate spectral separation between consecutive resonance peaks, thereby preventing undesired overlap between adjacent resonances. Further details regarding the adopted optimisation procedure and geometrical optimized dimensions can be found in Ref. [28].

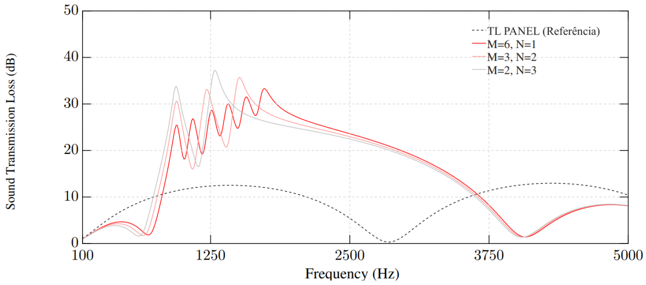

Fig. 11 – Sound Transmission Loss (STL) optimized at the reference resonance frequency for the configuration M = 6, N = 1. The red curve represents the STL predicted for the optimized AMM, while the dashed black line corresponds to the homogeneous reference panel

Perdita di trasmissione del suono (STL) ottimizzata alla frequenza di risonanza di riferimento per la configurazione M = 6, N = 1. La curva rossa rappresenta la STL prevista per l'AMM ottimizzato, mentre la linea nera tratteggiata corrisponde al pannello di riferimento omogeneo

In summary, this approach demonstrates the potential of systematically tuning the geometric design parameters to achieve enhanced sound attenuation over an extended target frequency range, thereby supporting an optimisation strategy aimed at maximising STL performance within a prescribed spectral interval. The resulting STL curve clearly illustrates the effectiveness of the proposed optimisation strategy, yielding a smooth and extended attenuation region with peak transmission loss values reaching approximately 20 dB. Although the parameter bounds were intentionally expanded beyond practical manufacturability limits, this procedure serves to highlight the intrinsic capability of the system when geometric constraints are relaxed.

The results demonstrate that the optimal geometric configurations for maximizing sound absorption and sound transmission loss are inherently different. This distinction arises from the underlying physical mechanisms governing each phenomenon. Sound absorption is primarily driven by impedance matching and critical coupling between the resonator system and the surrounding medium, whereas sound transmission loss is dominated by impedance mismatch and reflection mechanisms. Consequently, a configuration optimized for absorption does not necessarily provide optimal transmission loss performance, and vice versa. The proposed metamaterial panel should therefore be interpreted as a tunable system, where the geometrical parameters can be adjusted to prioritize a specific acoustic objective. This trade-off highlights the potential of the structure for multi-functional acoustic design, where application-specific requirements dictate the optimization strategy.

Overall, these findings support the development of advanced optimisation frameworks specifically tailored to maximise STL performance within predefined spectral ranges, while maintaining a clear pathway towards future manufacturable solutions.

4.3 | Architectural possibilities and design implications for building acoustics

Recognizing the substantial limitations associated with translating theoretical concepts into practical, manufacturable solutions at large scale, particularly when transferring laboratory-scale developments to real-world architectural applications, this challenge remains a critical barrier to implementation. This limitation is especially evident in the development of systems that can be integrated into building components without compromising constructability, structural integrity, or essential functional requirements.

This concluding section proposes goes beyond theoretical modelling but discusses the possible practical feasibility of a concept intentionally conceived with real building applications. Such multipurpose behaviour expands the architectural scenarios in which the panel can be applied, including:

- Reverberant spaces require improved low-frequency modal control.
- Ventilated interior partitions where a balance between absorption and insulation is required.
- Hybrid barrier–absorber systems integrated into building envelopes.

The acoustic performance observed in the present study may be directly associated with objective descriptors commonly used in architectural acoustics.

One of the possible applications is the proposition in internal rooms, as illustrated in Fig. 6(a), where the perfect sound absorption under subwavelength dimensions could promote significant damping and smoother low-frequency decay. These effects influence reverberation parameters such as T20 and T30, as well as the early-to-late energy ratio distribution [30]. Moreover, improved regulation of early reflections and mitigation of low-frequency modal build-up may enhance clarity indices C50 and C80, together with definition D50, especially in environments where excessive low-frequency energy masks transient acoustic information [30,31]. By attenuating noise within critical speech frequency bands, the proposed configuration may contribute to improved signal-to-noise ratios in occupied spaces. This aspect is particularly relevant for the Speech Transmission Index (STI), which is strongly affected by background noise levels and modulation transfer degradation [32].

The significative sound transmission loss capacity can be translated in façade-integrated barriers or ventilated systems, as illustrated in Fig. 6(b). Urban traffic noise is generally characterized by dominant energy content in the low- to mid-frequency range, with a substantial portion of its acoustic energy concentrated in the frequency range between 250 and 2500 Hz [33]. A spectral region in which traditional lightweight façade systems often exhibit limited performance unless substantial mass is introduced. As a result, the AMM can be dimensioned to target dominant traffic noise components without resorting to excessive surface mass or thickness. Furthermore, due to the open-channelled topology of the unit cell, the system preserves passive ventilation capability. This characteristic distinguishes it from conventional sealed barrier façades and aligns with contemporary trends in contemporary façade engineering and modular envelope systems concepts. In which increasingly moves beyond enclosure functions toward multifunctional components that mediate environmental exchanges while satisfying structural and comfort-driven criteria, including thermal, daylighting, and acoustic performance [34].

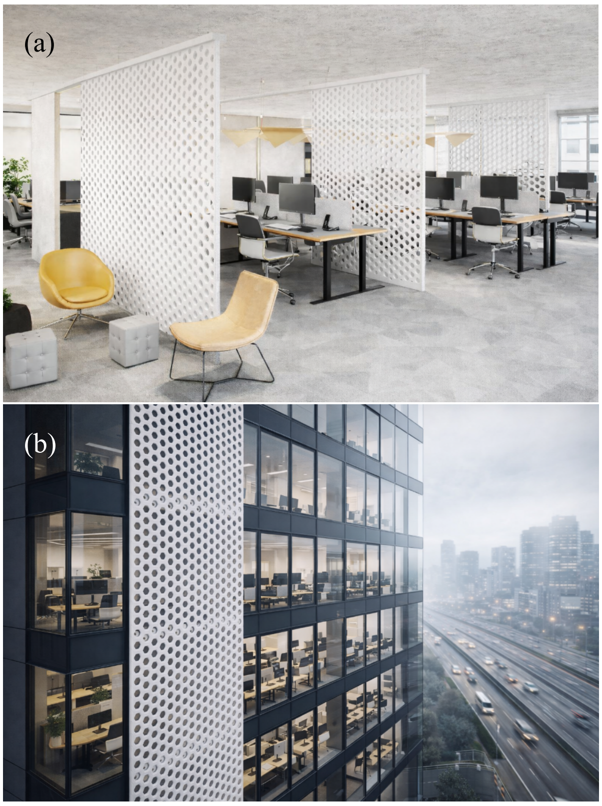

Fig. 12 – Illustrative representation of possible architectural applications of the proposed Hexagonal Acoustic Metamaterial. (a) Ventilated interior partitions where a balance between absorption and insulation is required. (b) Hybrid barrier-absorber systems integrated into building envelopes. Illustrative render "kindly" post-processed by an AI

Rappresentazione illustrativa delle possibili applicazioni architettoniche del metamateriale acustico esagonale proposto. (a) Partizioni interne ventilate dove è richiesto un equilibrio tra assorbimento e isolamento. (b) Sistemi ibridi barriera-assorbitore integrati negli involucri edilizi. Rendering illustrativo "gentilmente" post-elaborato da un'intelligenza artificiale

In addition to the objective acoustic performance discussed above, it is important to recognise that the successful integration of such systems into real building environments also depends on human perception and subjective acoustic comfort. Recent studies have highlighted the relevance of combining physical and psychoacoustic descriptors with soundscape-based evaluation methods, enabling a more comprehensive assessment of acoustic metamaterial applications in the built environment. In particular, the use of perceptual indicators such as pleasantness, calmness, and annoyance has been shown to provide meaningful insights into how users experience acoustically modified spaces, which may not be fully captured by traditional metrics such as absorption or transmission loss alone. Furthermore, soundscape-oriented methodologies, including questionnaire-based approaches and psychoacoustic analysis, have demonstrated their potential to bridge the gap between laboratory performance and real-world user experience. Therefore, future developments of the proposed system should consider the integration of perceptual evaluation frameworks, ensuring that the achieved acoustic performance is aligned with occupant comfort, usability, and overall environmental quality [35].

5 | Conclusions

The results obtained for the hexagonal acoustic metamaterial, formed by the association of Helmholtz resonators, demonstrate significant potential to evolve into a practical and lightweight solution, capable of operating at subwavelength dimensions and applicable to multiple acoustic contexts. Among its principal advantages, the proposed system was conceived with manufacturability in mind, while allowing the modular association of multiple units. In the context of civil engineering and architectural applications, however, large-scale production remains a critical challenge, primarily due to the limited availability and high cost of additive manufacturing processes when applied to this sector, despite their increasing consolidation in other engineering domains.

By exploiting the phenomenon of multiple coupled resonances combined with the local resonance effects of a simple and well-established acoustic device, namely the Helmholtz resonator, it was possible to develop a complex system capable of producing significant sound absorption responses, exceeding 80% of the incident acoustic energy. Furthermore, a broadband absorption performance of approximately 275Hz (from 325Hz to 600Hz) was achieved, resulting in a promising and efficient acoustic absorber. When considering its ability to interact with incident wavefronts in sound transmission scenarios, the preliminary investigations suggest the potential to extend the attenuation bandwidth to approximately 1200 Hz, with Sound Transmission Loss (STL) peaks reaching values close to 20 dB.

The findings presented herein support the development of optimization methodologies aimed at maximizing the acoustic performance of the system within prescribed spectral ranges. Such strategies may focus either on increasing attenuation levels, enhancing sound absorption capacity, or further extending the effective operational bandwidth of the system. Additionally, experimental validation through full-scale prototypes is strongly recommended, particularly using manufacturing techniques that offer improved cost-effectiveness, such as thermoplastic injection molding. Such investigations would allow a comprehensive assessment of practical manufacturing challenges, structural limitations, and overall feasibility.

In conclusion, although a several challenges remain in the conceptualization and scalability of acoustic metamaterials of this nature, the present study demonstrates the effectiveness of the proposed design, representing a further and meaningful step toward the practical implementation of acoustic metamaterials for noise mitigation purposes. The results provide additional insight into the design of manufacturable acoustic metamaterials and establish a consistent foundation for the development of composite structures suitable for applications in architectural acoustics and civil engineering.

Conclusioni

I risultati ottenuti per il metamateriale acustico esagonale, formato dall'associazione di risonatori di Helmholtz, dimostrano un potenziale significativo per evolversi in una soluzione pratica e leggera, in grado di operare a dimensioni sub-onda e applicabile a molteplici contesti acustici. Tra i suoi principali vantaggi, il sistema proposto è stato concepito tenendo conto della producibilità, consentendo al contempo l'associazione modulare di più unità. Nel contesto dell'ingegneria civile e delle applicazioni architettoniche, tuttavia, la produzione su larga scala rimane una sfida critica, principalmente a causa della limitata disponibilità e dell'elevato costo dei processi di produzione additiva applicati a questo settore, nonostante il loro crescente consolidamento in altri ambiti ingegneristici.

Sfruttando il fenomeno delle risonanze multiple accoppiate, combinato con gli effetti di risonanza locale di un dispositivo acustico semplice e consolidato, ovvero il risonatore di Helmholtz, è stato possibile sviluppare un sistema complesso in grado di produrre risposte di assorbimento acustico significative, superiori all'80% dell'energia acustica incidente. Inoltre, è stata raggiunta una prestazione di assorbimento a banda larga di circa 275 Hz (da 325 Hz a 600 Hz), dando vita a un assorbitore acustico promettente ed efficiente. Considerando la sua capacità di interagire con i fronti d'onda incidenti in scenari di trasmissione sonora, le indagini preliminari suggeriscono il potenziale per estendere la larghezza di banda di attenuazione a circa 1200 Hz, con picchi di perdita di trasmissione sonora (STL) che raggiungono valori prossimi a 20 dB.

I risultati presentati nel presente documento supportano lo sviluppo di metodologie di ottimizzazione volte a massimizzare le prestazioni acustiche del sistema entro intervalli spettrali prescritti. Tali strategie possono concentrarsi sull'aumento dei livelli di attenuazione, sul miglioramento della capacità di assorbimento acustico o sull'ulteriore estensione della larghezza di banda operativa effettiva del sistema. Inoltre, si raccomanda vivamente la validazione sperimentale tramite prototipi in scala reale, in particolare utilizzando tecniche di produzione che offrano un migliore rapporto costi-benefici, come lo stampaggio a iniezione termoplastico. Tali indagini consentirebbero una valutazione completa delle sfide pratiche di produzione, dei limiti strutturali e della fattibilità complessiva.

In conclusione, sebbene permangano diverse sfide nella concettualizzazione e nella scalabilità di metamateriali acustici di questa natura, il presente studio dimostra l'efficacia del progetto proposto, rappresentando un ulteriore e significativo passo avanti verso l'implementazione pratica di metamateriali acustici per scopi di mitigazione del rumore. I risultati forniscono ulteriori approfondimenti sulla progettazione di metamateriali acustici producibili e stabiliscono una base solida per lo sviluppo di strutture composite adatte ad applicazioni in acustica architettonica e ingegneria civile.

6 | Acknowledgements

"This work was supported by FCT/MCTES under the R&D Unit Institute for Sustainability and Innovation in Structural Engineering (ISISE), under the references UID/4029/2025 (https://doi.org/10.54499/UID/04029/2025) and UID/PRR/04029/2025 (https://doi.org/10.54499/UID/PRR/04029/2025), and under the Associate Laboratory Advanced Production and Intelligent Systems ARISE under reference LA/P/0112/2020 (https://doi.org/10.54499/LA/P/0112/2020)". The first author also acknowledges all the members of the Acoustics Research Group of the Engineering Department of the University of Ferrara for their support and hospitality during the period in which this research was developed.

Bibliography

[1] Doak PE. Excitation, transmission and radiation of sound from source distributions in hard-walled ducts of finite length (II): The effects of duct length. J Sound Vib 1973;31:137–74. https://doi.org/10.1016/S0022-460X(73)80372-4.

[2] Tijdeman H. On the propagation of sound waves in cylindrical tubes. J Sound Vib 1975;39:1–33. https://doi.org/10.1016/S0022-460X(75)80206-9.

[3] Zhang X, Qu Z, Wang H. iScience ll Engineering Acoustic Metamaterials for Sound Absorption : From Uniform to Gradient Structures. IScience 2020;23:101110. https://doi.org/10.1016/j.isci.2020.101110.

[4] Kumar S, Lee HP. Recent Advances in Active Acoustic Metamaterials Recent Advances in Active Acoustic Metamaterials 2020. https://doi.org/10.1142/S1758825119500819.

[5] Yu X, Lu Z, Liu T, Cheng L, Zhu J, Cui F. Sound transmission through a periodic acoustic metamaterial grating. J Sound Vib 2019;449:140–56. https://doi.org/10.1016/j.jsv.2019.02.042.

[6] Akl W, Baz A. Active control of the dynamic density of acoustic metamaterials. Applied Acoustics 2021;178:108001. https://doi.org/10.1016/j.apacoust.2021.108001.

[7] Liu Y, Xu W, Chen M, Yang T, Wang K, Huang X, *et al.* Three-dimensional fractal structure with double negative and density-near-zero properties on a subwavelength scale. Mater Des 2020;188:108470. https://doi.org/10.1016/j.matdes.2020.108470.

[8] Cox T, D'Antonio P. Acoustic Absorbers and Diffusers. CRC Press; 2016. https://doi.org/10.1201/9781315369211.

[9] Zieliński TG, Dauchez N, Boutin T, Leturia M, Wilkinson A, Chevillotte F, *et al.* Taking advantage of a 3D printing imperfection in the development of sound-absorbing materials.

Applied Acoustics 2022;197. https://doi.org/10.1016/j.apacoust.2022.108941.

[10] Zieliński TG, Chevillotte F, Deckers E. Sound absorption of plates with micro-slits backed with air cavities: Analytical estimations, numerical calculations and experimental validations. Applied Acoustics 2019;146:261–79. https://doi.org/10.1016/j.apacoust.2018.11.026.

[11] Fang N, Xi D, Xu J, Ambati M, Srituravanich W, Sun C, *et al.* Ultrasonic metamaterials with negative modulus. Nat Mater 2006;5:452–6. https://doi.org/10.1038/nmat1644.

[12] Červenka M, Bednařík M. Optimized compact wideband reactive silencers with annular resonators. J Sound Vib 2020;484. https://doi.org/10.1016/j.jsv.2020.115497.

[13] Lee SH, Park CM, Seo YM, Wang ZG, Kim CK. Acoustic metamaterial with negative modulus. Journal of Physics Condensed Matter 2009;21. https://doi.org/10.1088/0953-8984/21/17/175704.

[14] Lan J, Li Y, Yu H, Li B, Liu X. Nonlinear effects in acoustic metamaterial based on a cylindrical pipe with ordered Helmholtz resonators. Phys Lett A 2017;381:1111–7. https://doi.org/10.1016/j.physleta.2017.01.036.

[15] Jena DP, Dandsena J, Jayakumari VG. Demonstration of effective acoustic properties of different configurations of Helmholtz resonators. Applied Acoustics 2019;155:371–82. https://doi.org/10.1016/j.apacoust.2019.06.004.

[16] Jiménez N, Romero-García V, Pagneux V, Groby JP. Rainbow-trapping absorbers: Broadband, perfect and asymmetric sound absorption by subwavelength panels for transmission problems. Sci Rep 2017;7:1–12. https://doi.org/10.1038/s41598-017-13706-4.

[17] Jiménez N, Cox TJ, Vicent R, Groby J. Metadiffusers : Deep-subwavelength sound diffusers 2017. https://doi.org/10.1038/s41598-017-05710-5.

[18] Kumar S, Xiang TB, Lee HP. Ventilated acoustic metamaterial window panels for simultaneous noise shielding and air circulation. Applied Acoustics 2020;159:107088. https://doi.org/10.1016/j.apacoust.2019.107088.

[19] Kim SH, Lee SH. Air transparent soundproof window. AIP Adv 2014;4. https://doi.org/10.1063/1.4902155.

[20] Arjunan A, Baroutaji A, Robinson J, Vance A, Arafat A. Acoustic metamaterials for sound absorption and insulation in buildings. Build Environ 2024;251. https://doi.org/10.1016/j.buildenv.2024.111250.

[21] Rubino C, Liuzzi S, Fusaro G, Martellotta F, Scrosati C, Garai M. Balancing ventilation and sound insulation in windows by means of metamaterials: A review of the state of the art. Build Environ 2025;275. https://doi.org/10.1016/j.buildenv.2025.112780.

[22] Ramos D, Pompoli F, Marescotti C, Godinho L, Amado-Mendes P, Mareze P. Modelling the effective sound propagation properties of a hexagonal acoustic metamaterial using a dissipative equivalent-fluid approach under different termination conditions. J Sound Vib 2025;598. https://doi.org/10.1016/j.jsv.2024.118855.

[23] Dell A, Krynkin A, Horoshenkov K V. The use of the transfer matrix method to predict the effective fluid properties of acoustical systems. Applied Acoustics 2021;182:108259. https://doi.org/10.1016/j.apacoust.2021.108259.

[24] Jiménez N, Groby JP, Romero-García V. The Transfer Matrix Method in Acoustics: Modelling One-Dimensional Acoustic Systems, Phononic Crystals and Acoustic Metamaterials. vol. 143. Springer International Publishing; 2021. https://doi.org/10.1007/978-3-030-84300-7_4.

[25] ISO. 10534-2:1998 Acoustics, Determination of sound absorption coefficient and impedance in impedance tubes — Part 2: Transfer-function method 1998;1998.

[26] ASTM E2611. Standard Test Method for Measurement of Normal Incidence Sound Transmission of Acoustical Materials Based on the Transfer Matrix Method. ASTM International 2009:1–14. https://doi.org/10.1520/E2611-09.2.

[27] Ramos D, Godinho L, Amado-Mendes P, Mareze P. Broadband low-frequency bidimensional honeycomb lattice metastructure based on the coupling of subwavelength resonators. Applied Acoustics 2022;199. https://doi.org/10.1016/j.apacoust.2022.109038.

[28] Riccelli Del Teto Ramos D, Luís Manuel Cortesão Godinho P, Paulo Jorge Rodrigues Amado-Mendes P, Paulo Henrique Mareze P. STUDY AND DEVELOPMENT OF ACOUSTIC SOLUTIONS BASED ON ACOUSTIC METAMATERIAL CONCEPTS FOR THE CORRECTION OF VENTILATED ELEMENTS ON BUILDING FACADES. n.d.

[29] Fusaro G, Barbaresi L, Cingolani M, Garai M, Ida E, Prato A, *et al.* Investigation of the impact of additive manufacturing techniques on the acoustic performance of a coiled-up resonator. J Acoust Soc Am 2023;153:2921. https://doi.org/10.1121/10.0019474.

[30] Kuttruff H. Room Acoustics. CRC Press; 2002. https://doi.org/10.1201/9781482286632.

[31] Barron M. The subjective effects of first reflections in concert halls—The need for lateral reflections. J Sound Vib 1971;15:475–94. https://doi.org/10.1016/0022-460X(71)90406-8.

[32] Hou B, Wang L, Zeng Q, Mo J, Zhao W. Optimization strategies for enhancing speech intelligibility in underground platform public address systems. Build Environ 2025;280:113107. https://doi.org/10.1016/j.buildenv.2025.113107.

[33] De Salis MHF, Oldham DJ, Sharples S. Noise control strategies for naturally ventilated buildings. Build Environ 2002;37:471–84. https://doi.org/10.1016/S0360-1323(01)00047-6.

[34] Fusaro G, Kang J, Chang WS. Effective soundscape characterisation of an acoustic metamaterial based window: A comparison between laboratory and online methods. Applied Acoustics 2022;193. https://doi.org/10.1016/j.apacoust.2022.108754.

[35] Böke J, Knaack U, Hemmerling M. State-of-the-art of intelligent building envelopes in the context of intelligent technical systems. Intelligent Buildings International 2019;11:27–45. https://doi.org/10.1080/17508975.2018.1447437.